Regular Article

PHYSICAL CHEMISTRY RESEARCH
Published by the
Iranian Chemical Society
www.physchemres.org
info@physchemres.org

***Phys. Chem. Res.**, Vol. 5, No. 3, 409-424, September 2017*
DOI: 10.22036/pcr.2017.72268.1341

Chemical Kinetics for Reaction of 5-Nitro-1H-benzo[d]imidazole to Produce 6-Nitro-1H-benzo[d]imidazole and Calculation of Heat Capacity of Activation

M. Mohammadi, S.L. Hashemi Dashtaki, S. Ramazani* and B. Karami

Department of Chemistry, Yasouj University, 7591874934, Yasouj, Iran

(Received 6 January 2017, Accepted 4 February 2017)

The kinetics and mechanism of the reaction of 5-nitro-1H-benzo[d] imidazole to produce 6-nitro-1H-benzo[d] imidazole is studied by employing hybrid meta-density functional theory. MPWBlK/6-31+G** level calculations are carried out to obtain energies, to optimize the geometries of all stationary points along the PES, and also to determine the harmonic vibrational frequencies. Two transition states (TS_1 and TS_2) and a chemically-energized intermediate (Int) are involved along the calculated potential energy surface. RRKM-TST is used to compute the temperature dependence of the rate constants, which are determined using nonlinear least-squares fitting at 273-1000 K. The Arrhenius plot for all reactions is shown positive temperature dependence. Thermodynamic parameters are also used to determine the stability and the extent of spontaneity of the reaction. The self-consistent reaction field (SCRF) associated with DFT-based energy, optimization, and frequency calculations are used to model systems in solution and to compare them with the rate constants in the gas and solvent (water) phases. The variations of activation energy in the temperature range (273-1000 K) are determined in the gas and solvent phases. The heat capacity of activation of reactions ($\partial E_a/\partial T$) are also reported which is temperature dependent and is significant in low temperature.

Keywords: Tautomerism, Rate constant, Tunneling effect, Heat capacity of activation, Kinetics

INTRODUCTION

Benzimidazole is a heterocyclic aromatic ring system which is formed from benzene and imidazole rings. Benzimidazole is also known as 1,3-benzodiazole [1] possessing either of acidic and basic characteristics. The NH group creates strong acidity and weak basic properties in benzimidazole compound. Another important characteristic of benzimidazole is the possibility of forming salts.

The benzimidazole is considered as a useful structural modification of bioactive heterocyclic compounds for production of pharmaceutical or biological products [2].

Of the nitrogen heterocycles explored for development of pharmaceutically important compounds, benzimidazole has shown relatively high biological activity. It is anti-HIV [3,4], anti-herpes (HSV-1) [5], anti-influenza [6], anti-fungal [7] and a Raf kinase inhibitor [8]. The most prominent benzimidazole compound in nature is N-ribosyldimethyl benzimidazole which serves as an axial ligand for cobalt in vitamin B_{12} [9]. The wide application of benzimidazole in agriculture and veterinary medicine as fungicides, and anthelminthic drugs, and their experimental use in cancer chemotherapy, has led to a detailed research on its mode of action [10].

Unsubstituted NH groups in benzimidazole exhibit fast prototropic tautomerism leading to produce equilibrium mixtures of asymmetrically substituted compounds [11]. This reaction occurs through two hydrogen abstraction reactions which are equilibrium processes between T_1, T_2, and one intermediate. The NO_2 group on C_5 and nitrogen (N_2) close to the NO_2 group is different from the other nitrogen (N_9) atoms. In T_1 and T_2, H_{15} is connected to N_9 and N_2, respectively.

Tautomerism is a hydrogen rearrangement wherein

*Corresponding author. E-mail: ramazani@yu.ac.ir

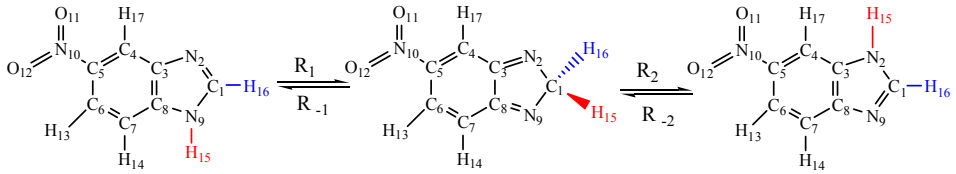

5-nitro-1*H*-benzo[*d*]imidazole (T_1) Intermediate (Int) 6-nitro-1*H*-benzo[*d*]imidazole (T_2)

hydrogen at one position migrates to the other positions of molecule. Since the energy difference between some tautomers is very small, the thermal energy shows a simple transfer from one tautomer to another at room temperature. In these kinds of reactions tunneling is also significant because a small atom (hydrogen) at low temperatures is transferred [12].

The current work is a sigmatropic hydrogen shifts or a hydrogen transfer reaction that plays an important role in some biologically relevant processes. Accordingly, theoretical study of the tautomerism of 5-nitro-1H-benzo[d] imidazole to produce 6-nitro-1H-benzo[d] imidazole in the gas and solvent (water) phases is considered to investigate their order of stability and to study the kinetics of the reactions.

The kinetics of four reactions are examined, along with the consumption of T_1 to produce T_2 and a chemically-energized intermediate (Int) and of T_2 to produce T_1 and Int as well. The potential energy surface (PES) is determined for these reactions along with the stationary points (intermediate and transition states) on the PES. Information about PES are used to report the kinetics and thermodynamics of the reaction. The hydrogen abstraction reaction makes the tunneling effect of this tautomerism very important for the calculation of rate constants.

ELECTRONIC STRUCTURE CALCULATIONS

In this study meta hybrid density functional theory (MPWBlK/6-31+G**) [13] method is employed for the kinetics study. The corresponding calculations are carried out using Gaussian 03 [14]. The geometries of all stationary points in the gas and solvent phases are optimized at the MPWBlK/6-31+G** level; (see Fig. 1). Harmonic vibrational terms are analytically computed at this level to characterize the stationary points as local minima (all frequencies are real) or first-order saddle points (only one imaginary frequency) and to obtain zero-point vibration energy corrections. The self-consistent reaction field (SCRF) [15] is used with DFT energy, optimization, and frequency calculations to model the systems in the solution. This information is used to calculate the vibrational partition function along the minimum energy path (MEP) and the ground state vibrational adiabatic potential curve. The energy values of all species are corrected for the zero-point energy. The harmonic vibrational frequency and moment of inertia for all stationary points are presented in Table S1 (supporting information). All frequencies are scaled by a factor of 0.951 [16].

RESULTS AND DISCUSSION

PES and Reaction Mechanism

The study of reactive chemical processes on a molecular level requires knowledge of the PES for the system considered. The nature of PES can be probed either experimentally or by quantum chemical calculations. The transition states are restricted subject to intrinsic reaction coordinate (IRC) [17,18] calculations to facilitate the connection with the minima along the reaction paths. Each IRC terminated upon reaching a minimum according to the default criterion. A one-dimensional PES for the path of conversion of T_1 to T_2 (Fig. 2) is reported. The PES is also used to calculate the barrier energy of the reaction. PES is involved T_1, T_2, two transition states (TS_1 and TS_2) and a chemically energized intermediate (Int). The difference between these molecules is the position of H_{15}. According to the PES in T_1, N_3 abstracts H_{15} on N_1 to produce T_2. This process is the tautomerism of 5-nitro-1H-benzo [d] imidazole and involves two channels (R_1 and R_2).

The intermediate is more unstable than T_1 and T_2

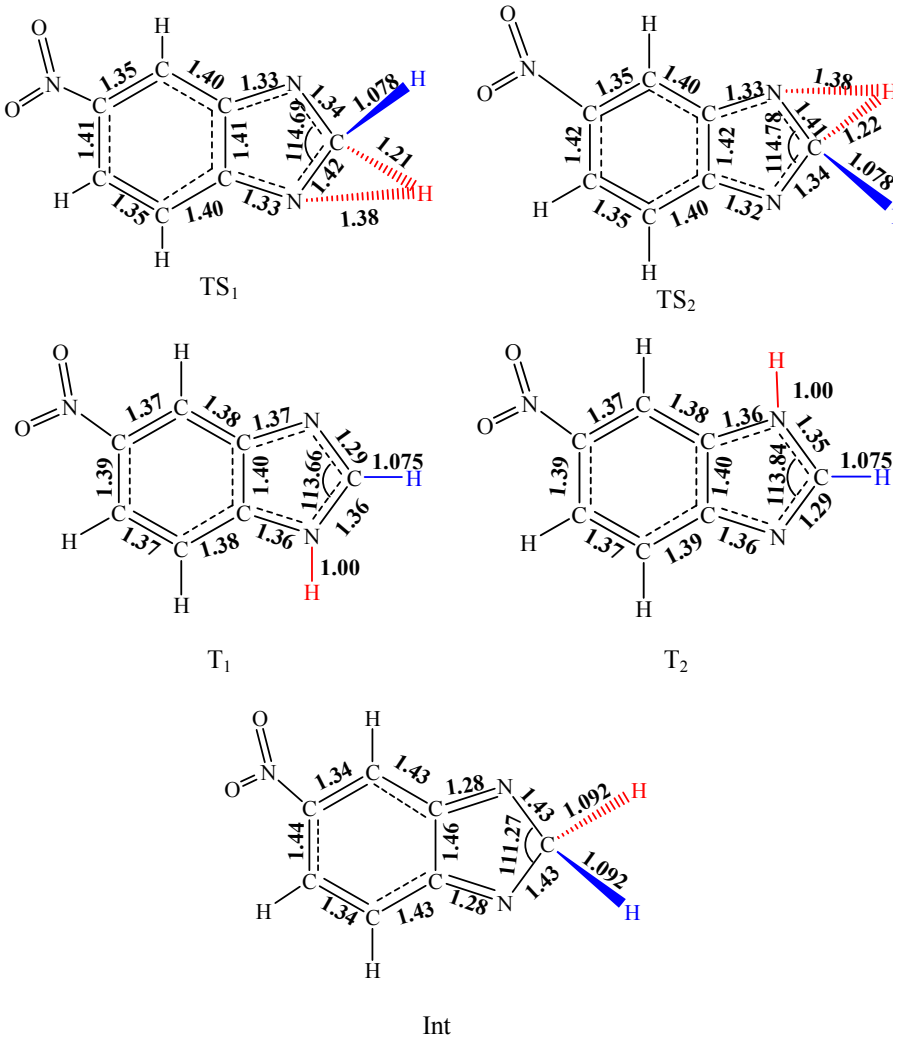

Fig. 1. Optimized structures of reactant, product, intermediate, TS_1 and TS_2 at MPWBlK/6-31+G** level.

because there is a mobility of Π electrons between five atoms (C_1, N_2, C_3, C_8 and N_9) in the pentagonal ring of T_1 and T_2. The resonance in the intermediate is between only four atoms (N_2, C_3, C_8 and N_9). The large bond lengths of C_1-N_2 and C_1-N_9 in Int than those in T_1 and T_2 also indicate this instability.

In the R_1 reaction, T_1 is converted to a chemically-energized intermediate (Int). C_2 abstracts H_{15} from N_9 to produce Int *via* TS_1. In the gas phase, TS_1 has an imaginary stretching frequency (1427.7i) in the plane ring (N_9-H_{15}→C_1) that corresponds to the reaction path. TS_1 has 242.5 and 83.5 kJ mol^{-1} energy more than T_1 and Int, respectively. These are the barrier energies of R_1 and R_{-1} in the gas phase. In the solvent phase, these values correspond to 287.0 and 97.0 kJ mol^{-1}, respectively, which are greater than those for gas phase.

As demonstrated in Table S4, there is no difference between H_{15} and H_{16}. In the R_2 reaction, N_2 abstracts H_{15} or H_{16} from C_1 in the intermediate to produce T_2. TS_2 has an imaginary frequency (1412.9i) indicating the reaction path frequency (C_1-H_{15}→N_2) of the connection of Int to T_2. TS_2 has 240.0 and 80.5 kJ mol^{-1} more energy than T_2 and Int, respectively; these are the barrier energies for R_{-2} and R_2, respectively, that correspond to 281.4 and 93.2 kJ mol^{-1} in

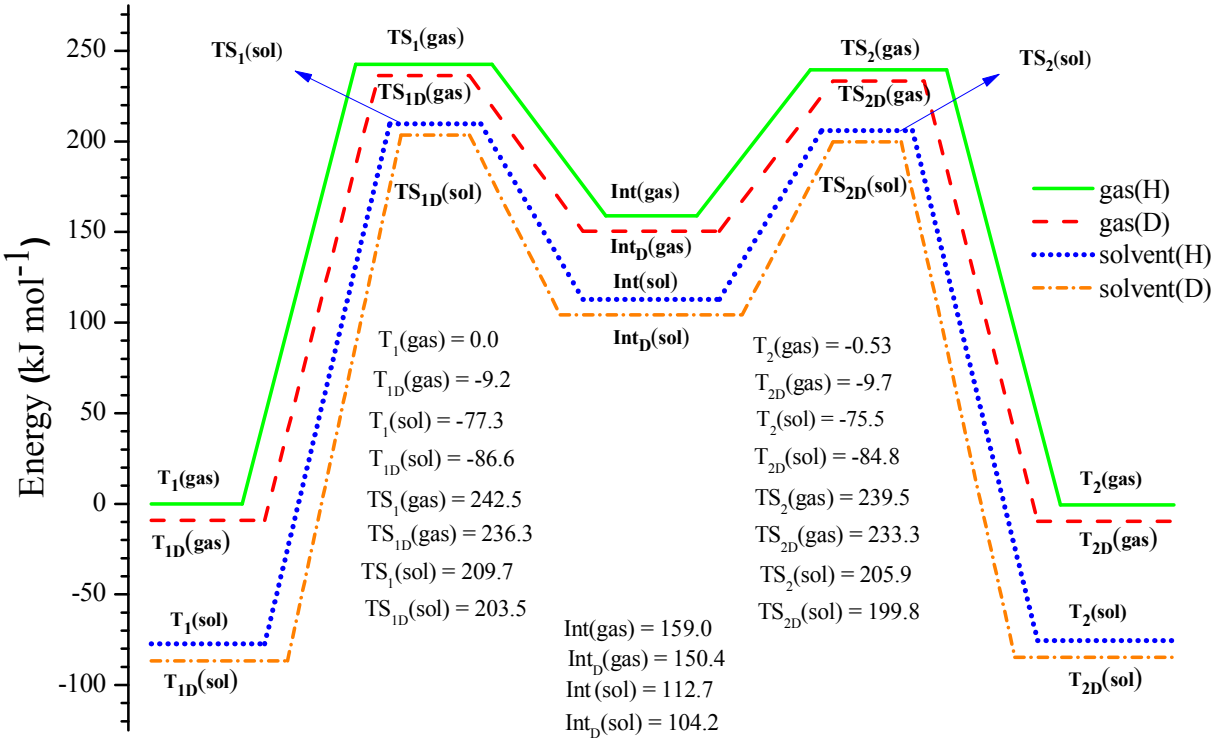

Fig. 2. The relative energies of stationary points in kJ mol^{-1} at the MPWBlK/6-31+G** level. All energy values are corrected by ZPE (zero point energy).

the solvent phase.

NBO Charge Distribution

As an additional tool to describe the electronic structure, natural bond orbital (NBO) analysis is utilized to investigate the atomic charge distribution and perform population analysis (Fig. 3). The NBO results can also be beneficial to understand the resonance and stability of T_1 and T_2. There is no significant difference between NBO charges of T_1 and T_2. In these two tautomers, NO_2 group is rather an acceptor, while NBO charges of the two nitrogen atoms of 5-membered ring depend upon whether hydrogen atom is connected to the nitrogen or not. The nitrogen atom which hydrogen is connected to is more negative than the other by ~0.1 electron. However, NBO charges of these two nitrogens are almost identical in the intermediate, and more positive than their charges in T_1 and T_2. In the intermediate structure, the negative charge is imposed to the outer carbon, resulting in negative NBO charge as opposed to its positive charge in T_1 and T_2.

Rate Constant Calculation

As previously mentioned, the tautomerism studies combine two steps. The intermediate can be expressed as vibrationally excited/vibration excitation. Where superscript "*" denotes the vibrationally-excited intermediate, ω is the rate constant for the stability of the excited molecules to produce unexcited intermediates. $k(\omega_1)$ and $k(\omega_2)$ are the rate constants of the reactions of $(T_1 \leftrightarrow Int^* \leftrightarrow Int)$ and $(T_2 \leftrightarrow Int^* \leftrightarrow Int)$, respectively.

RRKM-TST model [19-22] is used to calculate the individual rate constants. Steady-state approximation for the chemically activated intermediates (Int) is used to drive the following expression for an overall rate constant. This kind of treatment is considered to calculate the rate constants and relies on strong collision assumption causing an overestimation of the rate of collisional stabilization of the intermediates. Due to the hydrogen abstraction reaction in this tautomerism, tunneling effect is a very important factor that should be considered in the calculation of rate constants.

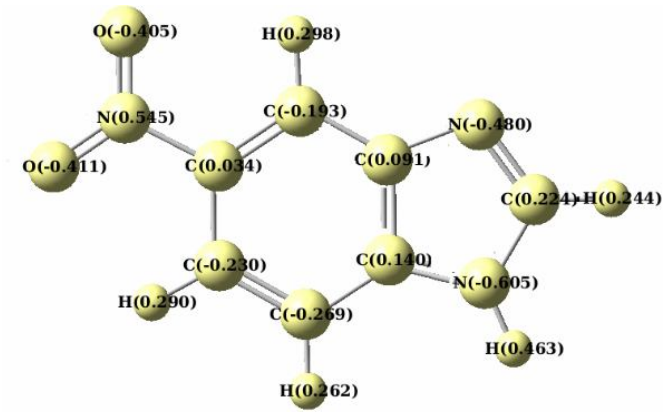

T_1

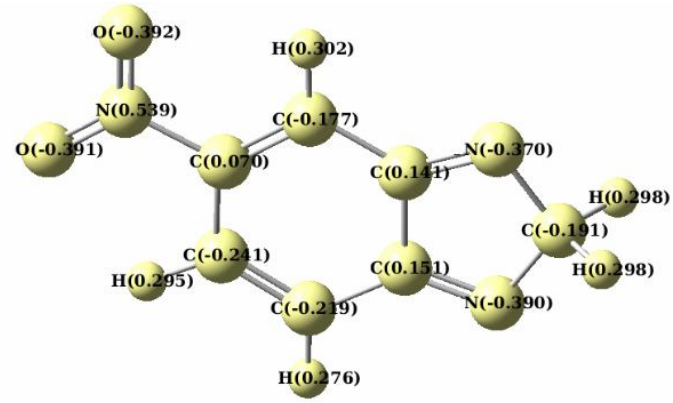

Int

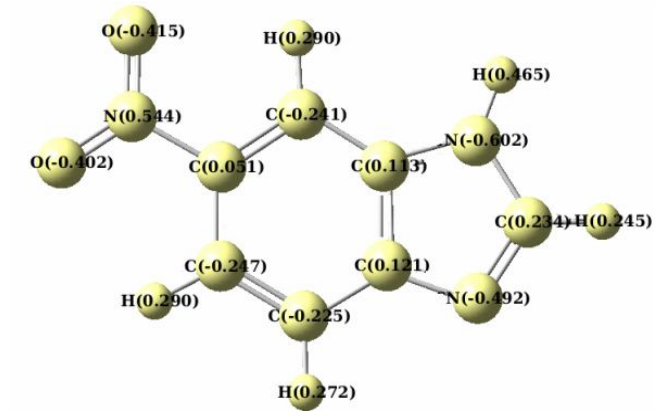

T_2

Fig. 3. NBO atomic charge of T_1, Int, and T_2 at the MPWBlK/6-31+G** level.

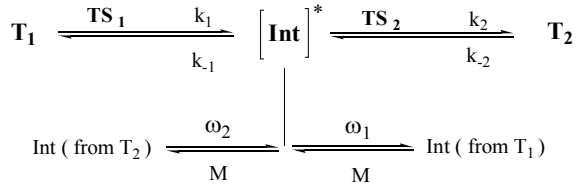

$$k(T1 \rightarrow T2) = \Gamma \frac{\sigma B_e Q_{TS_1^{\neq}}}{hQ_{T1}} \exp\left(\frac{-Ea}{RT}\right) \int_0^{\infty} \frac{k_2(\varepsilon)\{G(E_v^+)\} \exp\left(\frac{-E^+}{RT}\right)}{(\omega_1 + k_{-1}(\varepsilon) + k_2(\varepsilon))} dE^+ \quad (1)$$

$$k(T2 \rightarrow T1) = \Gamma \frac{\sigma B_e Q_{TS_2^{\neq}}}{hQ_{T2}} \exp\left(\frac{-Ea}{RT}\right) \int_0^{\infty} \frac{k_{-1}(\varepsilon)\{G(E_v^+)\} \exp\left(\frac{-E^+}{RT}\right)}{(\omega_2 + k_{-1}(\varepsilon) + k_2(\varepsilon))} dE^+ \quad (2)$$

$$k(\omega_1) = \Gamma \frac{\sigma B_e Q_{TS_1^{\neq}}}{hQ_{T1}} \exp\left(\frac{-Ea}{RT}\right) \int_0^{\infty} \frac{\omega_1\{G(E_v^+)\} \exp\left(\frac{-E^+}{RT}\right)}{(\omega_1 + k_{-1}(\varepsilon) + k_2(\varepsilon))} dE^+ \quad (3)$$

$$k(\omega_2) = \Gamma \frac{\sigma B_e Q_{TS_2^{\neq}}}{hQ_{T2}} \exp\left(\frac{-Ea}{RT}\right) \int_0^{\infty} \frac{\omega_2\{G(E_v^+)\} \exp\left(\frac{-E^+}{RT}\right)}{(\omega_2 + k_{-1}(\varepsilon) + k_2(\varepsilon))} dE^+ \quad (4)$$

where Γ is the tunneling factor, σ is the statistical factor (reaction path degeneracy), h is Plank's constant, $Q_{TS}^{\#}$ is the product of the translational and rotational partition functions of the transition states (TS_1 and TS_2), E_0 is the potential energy barrier for the entrance channel of intermediate formation (from T_1 and T_2) and is corrected for zero-point energy, E^+ is the total non-fixed energy of a given transition state, $G(E_{vr}^+)$ is the sum of the vibrational-rotational states of the transition states (TS_1 in the $T_1 \rightarrow T_2$ reaction and TS_2 in the $T_2 \rightarrow T_1$ reaction) at internal energy E_{vr}^+, ω ($Z\beta_c[A]$) is the collisional stabilization for Int for which β_c is the collision efficiency, and $k_x(\varepsilon)$ is the microcanonical rate coefficient for dissociation of intermediate in energy range ε to $\varepsilon + d\varepsilon$ and is calculated from the quotient of the sum of states to the density of states of the relevant step. Γ or Q_{tun} is calculated using the simple expression suggested by Shavitt. [22] as

$$Q_{tun} = 1 - \frac{1}{24}\left(\frac{h\nu_s}{k_B T}\right)^2 \left(1 + \frac{k_B T}{E_0}\right) \quad (5)$$

where ν_s is the imaginary frequency of the transition state at top of the barrier, k_B and h are the Boltzmann and Plank constants, respectively, and E_0 is the barrier height corrected for zero-point energy.

Figures 4-7 demonstrate the effect of temperature on the calculated rate constants for different channels in the gas and solvent phases in which $k(T_1 \rightarrow T_2)$, $k(T_2 \rightarrow T_1)$, $k(\omega_1)$, and $k(\omega_2)$ are the rate constants of reactions of production of T_2 from T_1, T_1 from T_2, Int from T_1, and Int from T_2, respectively. The value of barrier energies which have reported in Fig. 2 shows the difference between rates of various channels. In the gas phase, the rate constant for the reaction of (T_2 to produce T_1) is greater than that for the reaction ($T_1 \rightarrow T_2$) and the stabilization rates of the excited intermediates (ω_1 and ω_2). In the solvent phase, rate constant of reaction of $T_2 \rightarrow T_1$ is also greater than that for $T_1 \rightarrow T_2$. In Fig. 8, the ratio of the rate constants versus temperature is illustrated. As it is observed, at high temperatures, this ratio approaches to 1, indicating that the kinetics and rate constant for all reactions in the gas and solvent phases are similar. In addition, at low temperatures (below 310 K), the ratio of the rate constants in the gas and solvent phases are different and every reaction has an especial value. The effect of the solvent is evident for every reaction. Figure 8 illustrates that $k(T_1 \rightarrow T_2)$ is more dependent on the phase of the reaction than $k(T_2 \rightarrow T_1)$. Collisional stabilization rate constants $k(\omega_1)$ and $k(\omega_2)$ are also dependent on the phase of the reaction at low temperatures. Figure 9 shows the ratio of the rate constant in the gas and solvent phases and demonstrates the solvent effect in deuterium transfer reactions. For this reaction (D transfer), $k(\omega_1)$ and $k(\omega_2)$ have different values in the gas and solvent phases. In contrast, the reaction with a lower barrier energy is more sensitive to a temperature change.

The tunneling effect is significant because this tautomerism is combined from two hydrogen transfer

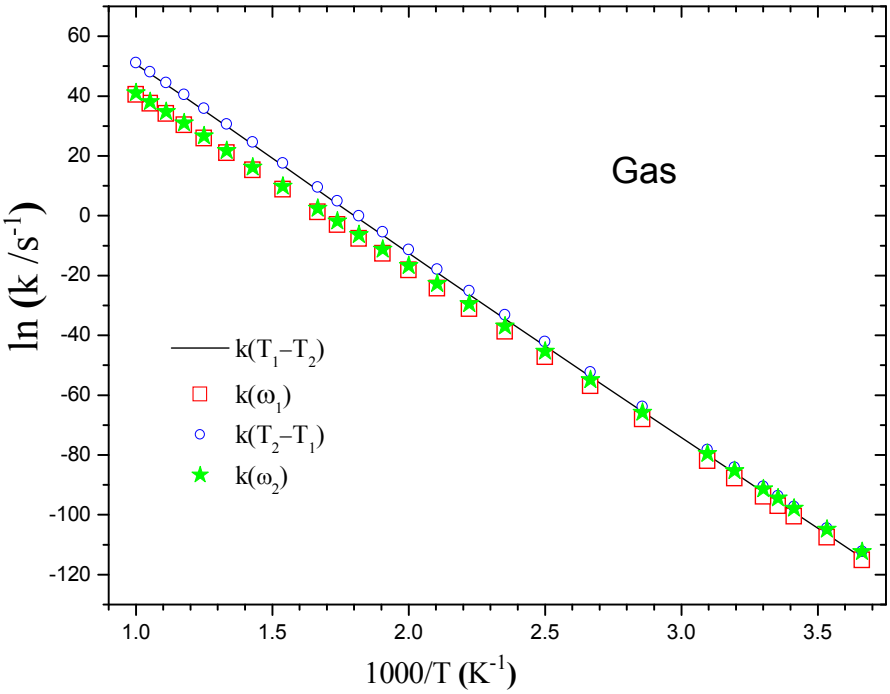

Fig. 4. Arrhenius plot of the calculated rate constants in the gas phase.

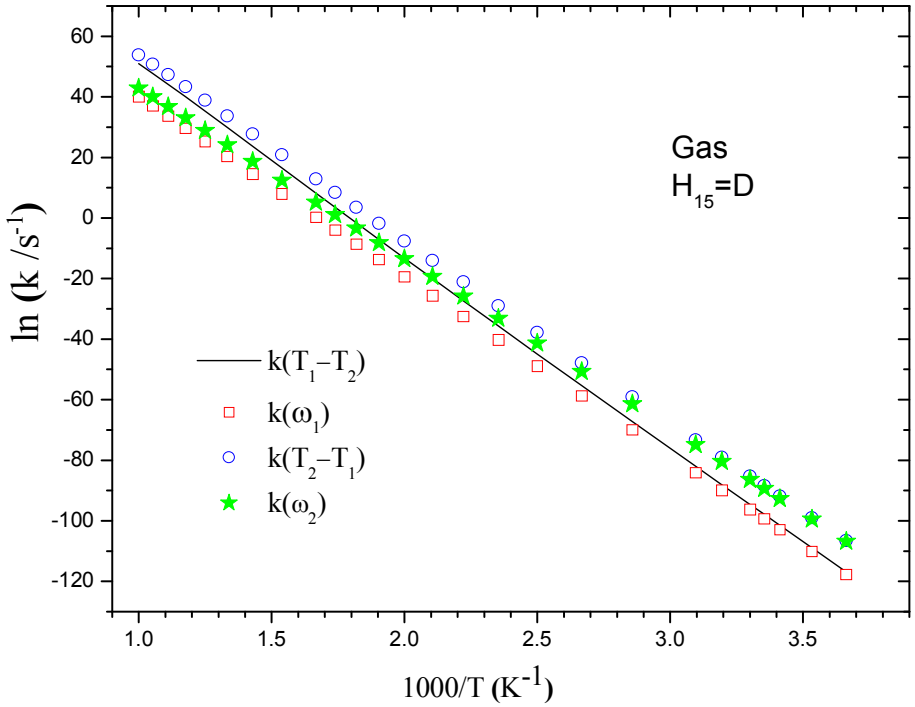

Fig. 5. Arrhenius plots of the calculated rate constants in the gas phase which H_{15} has been replaced with deuterium.

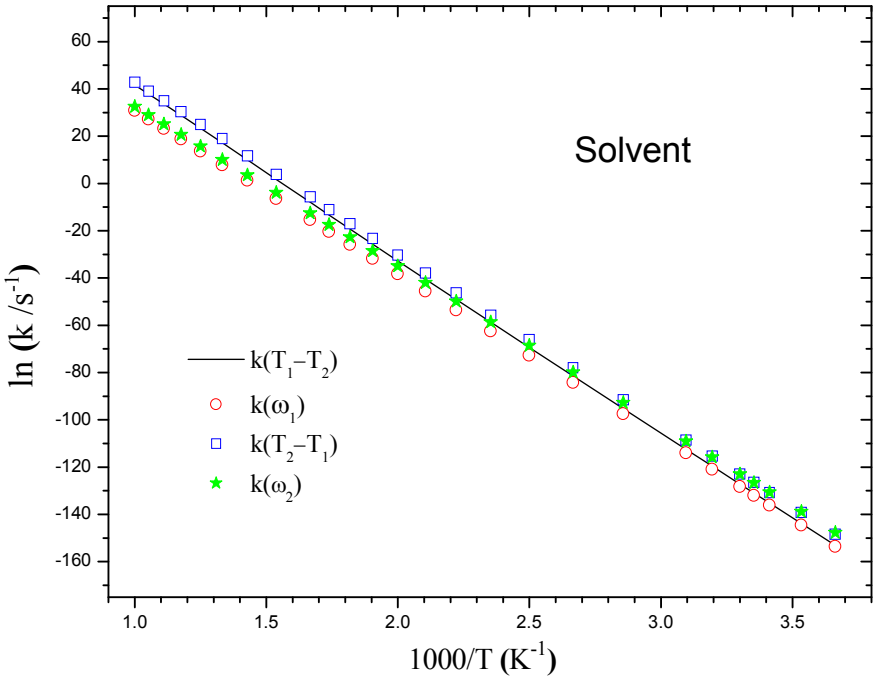

Fig. 6. Arrhenius plot of the calculated rate constants in solvent (water) phase.

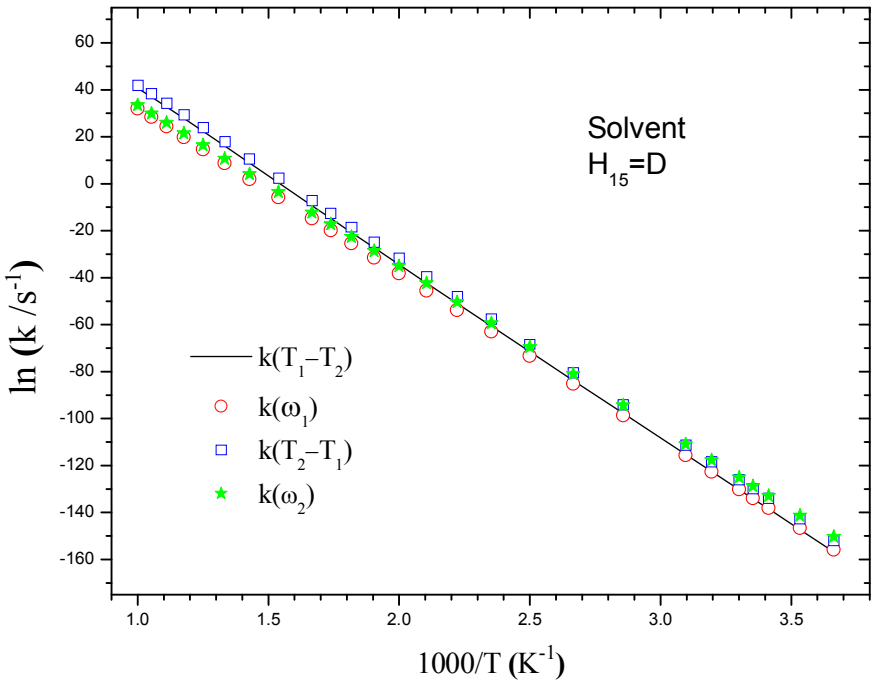

Fig. 7. Arrhenius plot of the calculated rate constants in solvent (water) phase which H_{15} has been replaced with deuterium.

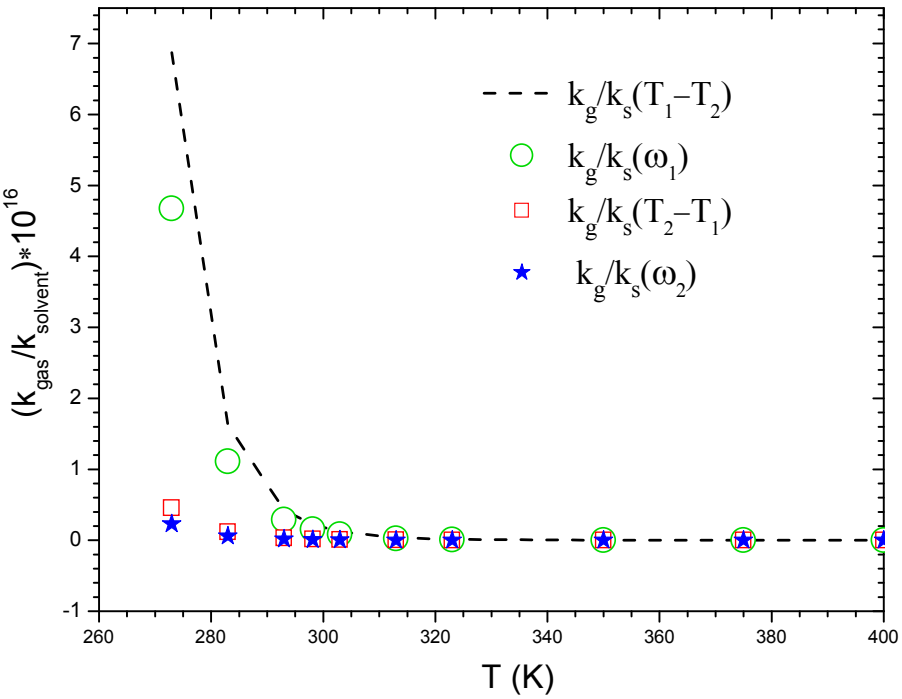

Fig. 8. Ratio of rate constants in the gas and solvent (water) phases for different reactions.

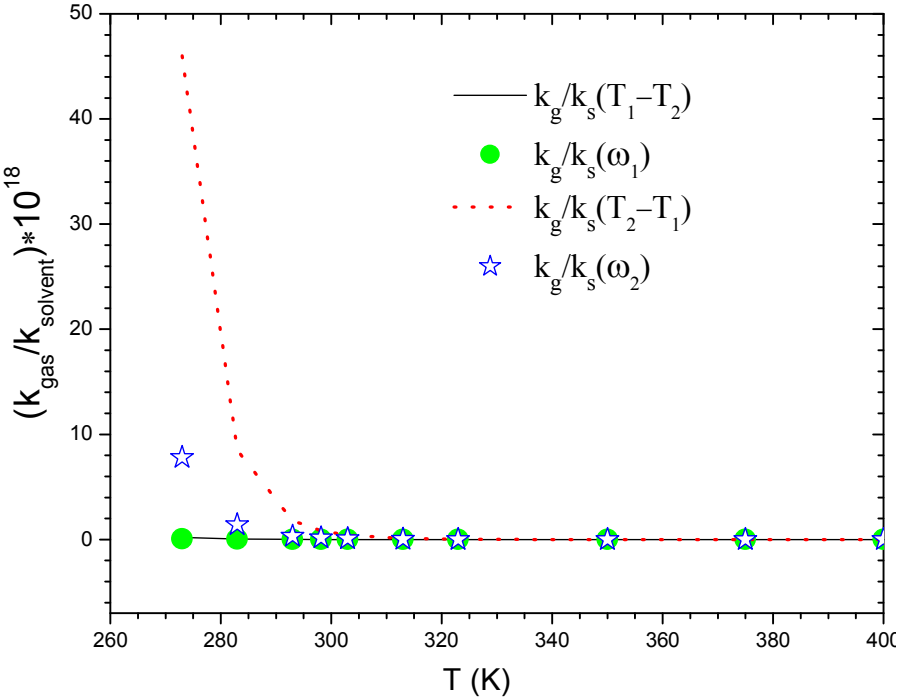

Fig. 9. Ratio of rate constants in the gas and solvent (water) phases for different reactions. H_{15} has been replaced with deuterium.

Table 1. Tunneling Factor (Γ) for all Reactions in the Gas Phase

	H				D			
T (K)	$T_1 \rightarrow T_2$	ω_1	$T_2 \rightarrow T_1$	ω_2	$T_1 \rightarrow T_2$	ω_1	$T_2 \rightarrow T_1$	ω_2
273	3.380	3.380	3.330	3.330	2.305	2.305	2.282	2.280
283	3.216	3.216	3.171	3.171	2.212	2.214	2.192	2.192
293	3.068	3.068	3.022	3.025	2.026	2.132	2.111	2.113
298	2.998	2.998	2.956	2.956	2.096	2.094	2.075	2.075
303	2.936	2.933	2.895	2.895	2.059	2.061	2.040	2.040
313	2.815	2.812	2.773	2.776	1.994	1.992	1.974	1.976
323	2.702	2.702	2.667	2.667	1.933	1.933	1.916	1.916
350	2.452	2.452	2.421	2.421	1.795	1.795	1.781	1.781
375	2.266	2.266	2.241	2.239	1.694	1.694	1.680	1.682
400	2.113	2.115	2.090	2.090	1.610	1.610	1.598	1.598
425	1.988	1.986	1.968	1.968	1.542	1.540	1.531	1.531
450	1.881	1.881	1.863	1.863	1.481	1.483	1.474	1.474
475	1.793	1.793	1.775	1.775	1.435	1.433	1.426	1.426
500	1.714	1.714	1.701	1.701	1.391	1.392	1.384	1.385
525	1.649	1.649	1.636	1.636	1.355	1.355	1.349	1.349
550	1.592	1.592	1.579	1.579	1.324	1.324	1.319	1.319
575	1.542	1.542	1.531	1.531	1.297	1.297	1.292	1.292
600	1.498	1.498	1.487	1.489	1.274	1.274	1.269	1.267
650	1.425	1.426	1.416	1.416	1.232	1.232	1.229	1.229
700	1.366	1.368	1.361	1.359	1.201	1.201	1.197	1.198
750	1.320	1.320	1.314	1.314	1.175	1.176	1.172	1.172
800	1.283	1.283	1.276	1.276	1.155	1.154	1.153	1.151
850	1.250	1.250	1.245	1.246	1.138	1.138	1.135	1.135
900	1.224	1.223	1.219	1.219	1.123	1.123	1.121	1.121
950	1.201	1.202	1.196	1.197	1.110	1.111	1.108	1.108
1000	1.182	1.182	1.178	1.178	1.100	1.099	1.099	1.097

Table 2. Tunneling Factor (Γ) for all Reactions in Solvent Phase

	H				D			
T (K)	$T_1 \rightarrow T_2$	ω_1	$T_2 \rightarrow T_1$	ω_2	$T_1 \rightarrow T_2$	ω_1	$T_2 \rightarrow T_1$	ω_2
273	3.146	3.146	3.077	3.080	2.293	2.293	2.257	2.257
283	2.995	2.998	2.936	2.933	2.203	2.206	2.171	2.168
293	2.863	2.866	2.807	2.804	2.123	2.123	2.092	2.092
298	2.801	2.801	2.743	2.743	2.085	2.085	2.054	2.054
303	2.743	2.743	2.689	2.689	2.050	2.050	2.020	2.022
313	2.633	2.635	2.583	2.583	1.984	1.984	1.956	1.956
323	2.537	2.537	2.487	2.487	1.925	1.925	1.898	1.900
350	2.309	2.309	2.268	2.268	1.788	1.790	1.766	1.766
375	2.140	2.140	2.104	2.104	1.689	1.687	1.667	1.667
400	2.002	2.004	1.972	1.972	1.605	1.605	1.587	1.587
425	1.889	1.889	1.863	1.861	1.536	1.536	1.520	1.520
450	1.795	1.793	1.770	1.770	1.478	1.478	1.465	1.465
475	1.714	1.713	1.690	1.690	1.429	1.429	1.418	1.418
500	1.644	1.644	1.623	1.624	1.388	1.388	1.377	1.377
525	1.586	1.586	1.567	1.565	1.351	1.353	1.342	1.342
550	1.533	1.534	1.516	1.516	1.322	1.320	1.311	1.311
575	1.489	1.487	1.473	1.473	1.294	1.293	1.287	1.287
600	1.449	1.449	1.435	1.435	1.270	1.270	1.262	1.262
650	1.383	1.383	1.372	1.370	1.231	1.230	1.225	1.224
700	1.330	1.331	1.320	1.319	1.200	1.198	1.194	1.194
750	1.289	1.288	1.279	1.280	1.174	1.174	1.169	1.169
800	1.254	1.254	1.246	1.245	1.153	1.153	1.148	1.148
850	1.225	1.225	1.218	1.218	1.135	1.135	1.132	1.131
900	1.201	1.201	1.195	1.195	1.122	1.122	1.119	1.117
950	1.181	1.181	1.175	1.175	1.108	1.110	1.106	1.106
1000	1.163	1.163	1.158	1.158	1.099	1.099	1.095	1.095

Table 3. The fitted Parameters Using $k(s^{-1}) = A(\frac{T}{300})^n \exp\left[-\frac{E(T+T_0)}{R(T^2+T_0^2)}\right]$ Arrhenius Equations for Reactions in the Temperature Range T = 273-1000 K

		A (s^{-1})	n	E (kJ mol^{-1})	T_0 (K)
k^H_{gas}	$T_1 \rightarrow T_2$	7.7×10^{37}	11.0	376.7	107.1
	ω_1	8.6×10^{31}	11.0	357.4	79.7
	$T_2 \rightarrow T_1$	8.3×10^{37}	11.0	372.8	106.9
	ω_2	7.1×10^{31}	11.0	353.5	74.5
$k^H_{solvent(water)}$	$T_1 \rightarrow T_2$	4.2×10^{35}	14.6	440.1	99.3
	ω_1	4.2×10^{30}	12.9	431.8	64.5
	$T_2 \rightarrow T_1$	6.7×10^{35}	14.4	431.8	99.4
	ω_2	1.9×10^{31}	12.2	425.5	61.2
k^D_{gas}	$T_1 \rightarrow T_2$	1.0×10^{37}	13.0	378.3	100.0
	ω_1	1.2×10^{31}	12.6	364.5	65.0
	$T_2 \rightarrow T_1$	1.6×10^{37}	13.0	359.6	100.0
	ω_2	6.3×10^{31}	11.9	349.6	58.8
$k^D_{solvent(water)}$	$T_1 \rightarrow T_2$	6.5×10^{35}	14.3	448.2	96.7
	ω_1	2.5×10^{32}	11.8	441.5	70.2
	$T_2 \rightarrow T_1$	1.2×10^{36}	14.1	440.1	97.0
	ω_2	7.5×10^{32}	11.2	433.6	69.0

reactions. The rate constants for tunneling are determined showing that the effect for $k(T_1 \rightarrow T_2)$ is more tangible than that for $k(T_2 \rightarrow T_1)$ (Tables 1 and 2). The primary kinetic isotope effect is used to better understand the kinetics of the reactions [23,24]. Replacement of hydrogen with deuterium increased the rate of the intermediate production from the exited intermediate $k(\omega_2)$ and $k(T_2 \rightarrow T_1)$ than ($k(\omega_1)$ and $k(T_1 \rightarrow T_2)$ (Fig. S1).

Nonlinear least-squares fitting technique [25] is used to calculate the rate constants at T = 273-1000 K for rate constants $k(s^{-1}) = A(\frac{T}{300})^n \exp\left[-\frac{E(T+T_0)}{R(T^2+T_0^2)}\right]$ (Table 3).

Activation energy is also calculated at T = 273-1000 K Using $E_a = E\frac{T^4 + 2T_0T^3 - T_0^3T}{(T^2+T_0^2)^2} + nRT$, where A, n, E and T_0 are fitting parameters, and R is the gas constant. Figure 10 illustrates the variation of activation energy in the temperature range T = 273-1000 for T1→T2 and T2→T1 in the gas and solvent phases. This variation is the result of non-Arrhenius behavior due to the tunneling effect in low temperatures. Activation energy of reactions in solvent phase is more sensitive to temperature changes than those in the gas phase. [It is better to use present passive verbs: In Fig. 11, slope of the curves in each point representing the

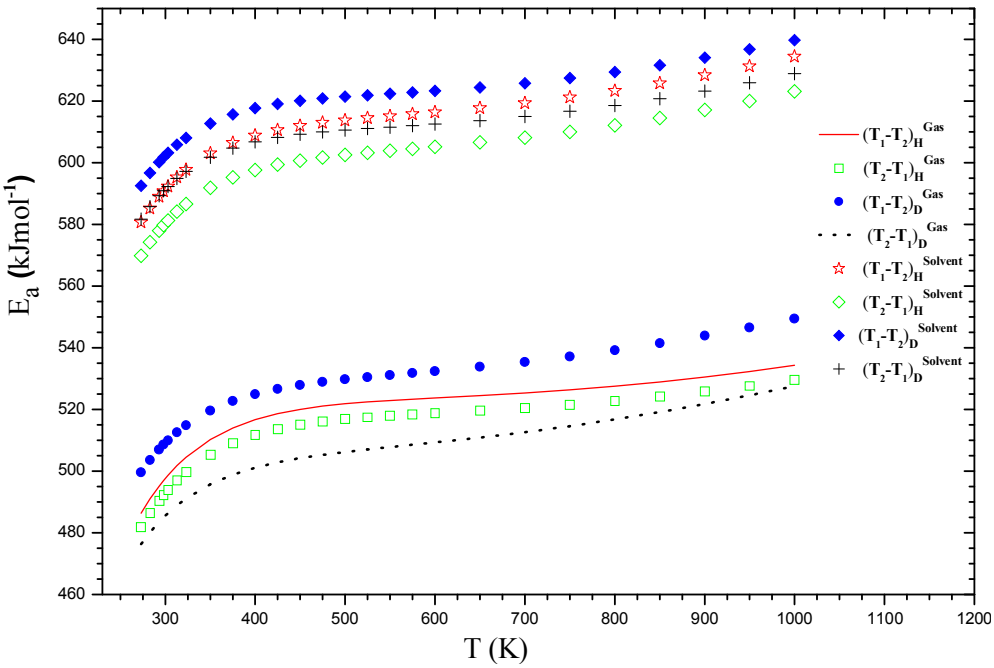

Fig. 10. Variation of activation energy in the temperature range T = 273-1000 K for $T_1 \rightarrow T_2$ and $T_2 \rightarrow T_1$ in the gas and solvent (water) phases.

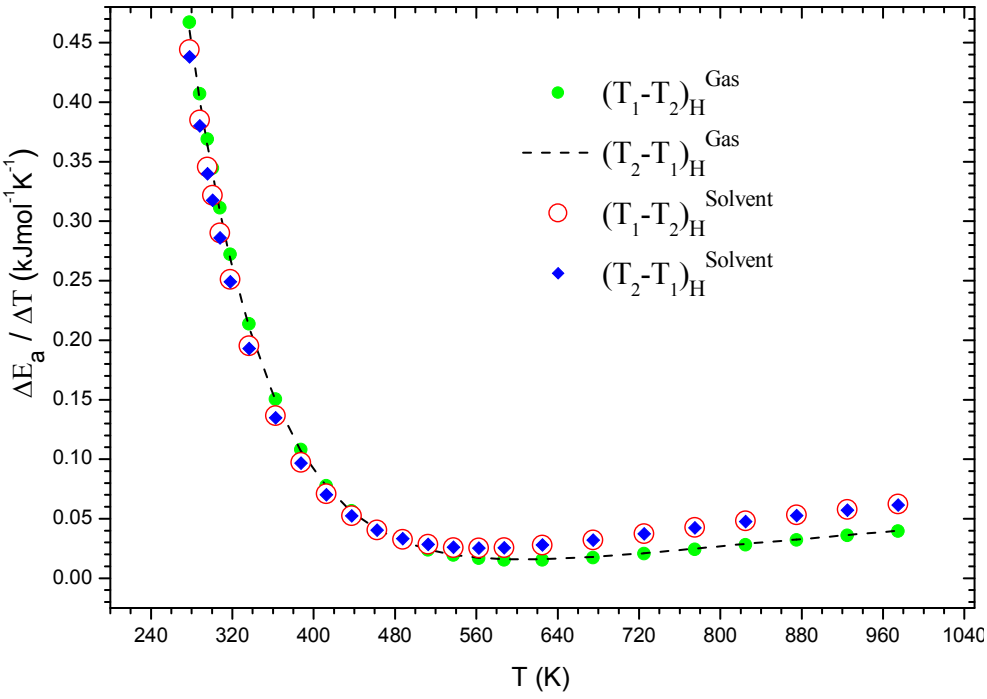

Fig. 11. Variation of heat capacity of activation energy in the temperature range T = 273-1000 K for $T_1 \rightarrow T_2$ and $T_2 \rightarrow T_1$ in the gas and solvent (water) phases.

Table 4. Relative Free Energy, Enthalpy, and Entropy Differences between Stationary Points and T_1 in the Gas Phase. The Numbers in Parentheses are the Corresponding Values in Solvent (Water) Phase (T = 298 K)

	ΔG (kJ mol^{1})	ΔH (kJ mol^{1})	ΔS J (mol^{-1} K^{-1})
T_1	0.00	0.00	0.00
Int	157.89(173.78)	159.55(176.18)	5.56(8.04)
T_2	-0.51(2.08)	-0.51 (2.00)	0.01(-0.29)
TS_1	242.34(255.63)	242.06(256.41)	-0.93(2.62)
TS_2	239.51(252.19)	239.01(252.63)	-1.66(1.47)
T_1(D)	0.00	0.00	0.00
Int (D)	158.50(174.40)	160.00(176.79)	5.02(8.03)
T_2(D)	-0.50(2.06)	-0.50(1.98)	0.03(-0.27)
TS_1(D)	245.54(258.83)	244.84(259.35)	-2.35(1.74)
TS_2(D)	242.71(255.39)	241.79(255.56)	-3.09(0.60)

heat capacity of activation of reaction ($\partial E_a/\partial T$) is shown. Figure 11 shows slope of the curve in each point (temperatures) presented as the heat capacity of activation of the reaction ($\partial E_a/\partial T$). This parameter at high temperatures is nearly constant and is greater than that at low temperatures.

Thermodynamic Calculations

Figure 1 shows a difference in the resonance in the structures of T_1, T_2 and intermediate in which the intermediate is much smaller than T_1 and T_2. The mobility of the Π electrons in the intermediate occurs between four atoms (N_2, C_3, C_8 and N_9) that is lower for T_1 and T_2, in which the Π electrons are localized between five atoms (C_1, N_2, C_3, C_8 and N_9). Table 4 and Fig. 2 show that T_1 and T_2 are much more stable than the intermediate because T_1 and T_2 exhibit high resonances. The stability of T_1 and T_2 are different in the gas and solvent phases. In the gas phase, T_2 is only 0.5 kJ mol^{-1} more stable than T_1; in the solvent phase, T_1 is 1.80 kJ mol^{-1} more stable than T_2. Moreover, in the gas and solvent phases, ΔG for the reactions of (T_1 to produce T_2) and (T_2 to produce T_1) have different signs. This indicates that $T_1 \rightarrow T_2$ reaction in the gas phase and $T_2 \rightarrow T_1$ in the solvent phase are spontaneous.

CONCLUSIONS

A two-step mechanism is used for discussion of reaction in this paper. The suggested mechanism consists of three stable molecules (T_1, T_2 and Int) and two transition states (TS_1 and TS_2). T_1 and T_2 are more stable than the intermediate. In the gas phase, T_2 is more stable than T_1 and in the solvent (water) phase *vice versa*. The thermodynamic parameters indicate that the process to produce T_1 and T_2 is spontaneous in the solvent and gas phases, respectively. RRKM rate constant calculations show that the reaction rate of T_2 to produce T_1 in the gas phase is greater than that in the reverse reaction; in the solvent phase the two reactions are comparable. At high temperatures, the rate constants in the gas and solvent phases are similar for all reactions. At

low temperatures (below 310 K), the ratio of rate constants in the gas and solvent phases are very different and have different values for every reaction. The solvent effect is also evident and different for every reaction. At low temperatures, because of the tunneling effect non-Arrhenius behavior is observed in reactions with high activation energy.

REFERENCES

[1] Agrawal, O. P., Organic Chemistry Reactions and Reagents, Goel publishing house, New Delhi:1996. pp. 627-628, 686-715.

[2] Verma, N.; Singh, R. B.; Srivastava, S.; Dubey, P., Benzimidazole: A plethro of biological load, *J. Chem. Pharm. Res.* **2016**, *8*, 365-374.

[3] Porcari, A. R.; Devivar, R. V.; Kucera, L. S.; Drach, J. C.; Townsend, L. B., Design, synthesis, and antiviral evaluations of 1-(substituted benzyl)-2-substituted-5,6-dichlorobenzimidazoles as nonnucleoside analogues of 2,5,6-trichloro-1-(beta-D-ribofuranosyl) benzimidazole, *J. Med. Chem.* **1998**, *41*, 1252-1262, DOI: 10.1021/jm970559i.

[4] Roth, T.; Morningstar, M. L.; Boyer, P. L.; Hughes, S. H.; Buckheitjr, R. W.; Michejda, C. J., Synthesis and biological activity of novel nonnucleoside inhibitors of HIV-1 reverse transcriptase. 2-Aryl-substituted benzimidazoles, *J. Med. Chem.* **1997**, *40*, 4199-4207, DOI: 10.1021/jm970096g.

[5] Migawa, M. T.; Girardet, J. L.; Walker, J. A.; Koszalka, G. W.; Chamberlain, S. D.; Drach, J. C.; Townsend, L. B., Design, synthesis, and antiviral activity of alpha-nucleosides: D- and L-isomers of lyxofuranosyl- and (5-deoxylyxofuranosyl) benzimidazoles, *J. Med. Chem.* **1998**, *41*, 1242-1251, DOI: 10.1021/jm970545c.

[6] Tamm, I., Ribonucleic acid synthesis and infulenza virus multiplication, *Science*. **1957**, *126*, 1235-1236.

[7] Kus, C., Synthesis of some new benzimidazole carbamate derivatives for evaluation of antifungal activity, *Turk. J. Chem.* **2003**, *27*, 35-39.

[8] Buchstaller, H. P.; Burgdorf, L.; Finsinger, D.; Stieber, F.; Sirrenberg, C.; Amendt, C.; Grell, M.; Zenke, F.; Krier, M., Design and synthesis of isoquinolines and benzimidazoles as REF kinase inhibitors, *Bioorg. Med. Chem. Lett*. **2011**, *21*, 2264-2269, DOI: 10.1016/j.bmcl.2011.02.108.

[9] Barker, H. A.; Smyth, R. D.; Weissbach, H.; Toohey, J. I.; Ladd, J. N.; Volcani, B. E., Isolation and properties of crystalline cobamide coenzymes containing benzimidazole or 5,6-dimethyl-benzimidazole, *J. Biol. Chem.* **1960**, *235*, 480-488.

[10] Davidse, L. C., Benzimidazole fungicides: mechanism of action and biological impact, *Ann. Rev. Phytopathol.* **1986**, *24*, 43-65, DOI: 10.1146/ annurev.py.24.090186.000355.

[11] Kalyankar, T. M.; Pekamwar, S. S.; Wadher, S. J.; Tiprale, P. S.; Shinde, G. H., Review on benzimidazole derivative, International Journal of Chemical and Pharmaceutical Sciences, International Journal of Chemical and Pharmaceutical Sciences. **2012**, *3*, 1-10.

[12] Mohammadi, M.; Ramazani, S.; Theoretical kinetics study of thymine tautomerism and interaction of Na_+ with its tautomer, *Molecular Physics.* **2016**, *114*, 3356-3374, DOI: 10.1080/00268976.2016.1232845.

[13] Zhao, Y.; Truhlar, D. G., Hybrid meta density functional theory methods for thermochemistry, thermochemical kinetics, and noncovalent interactions: the MPW1B95 and MPWB1K models and comparative assessments for hydrogen bonding and van der Waals interactions, *J. Phys. Chem.A.* 2004, *108*, 6908-6918, DOI: 10.1021/jp048147q CCC: $27.50.

[14] Frisch, M. J.; Trucks, G. W.; Schlegel, H. B.; Scuseria, G. E.; Robb, M. A.; Cheeseman, J. R.; Montgomery, J. A.; Jr., Vreven, T.; Kudin, K. N.; Burant, J. C.; Millam, J. M.; Iyengar, S. S.; Tomasi, J.; Barone, V.; Mennucci, B.; Cossi, M.; Scalmani, G.; Rega, N.; Petersson, G. A.; Nakatsuji, H.; Hada, M.; Ehara, M.; Toyota, K.; Fukuda, R.; Hasegawa, J.; Ishida, M.; Nakajima, T.; Honda, Y.; Kitao, O.; Nakai, H.; Klene, M.; Li, X.; Knox, J. E.; Hratchian, H. P.; Cross, J. B.; Bakken, V.; Adamo, C.; Jaramillo, J.; Gomperts, R.; Stratmann, R. E.; Yazyev, O.; Austin, A. J.; Cammi, R.; Pomelli, C.; Ochterski, J.

W.; Ayala, P. Y.; Morokuma, K.; Voth, G. A.; Salvador, P.; Dannenberg, J. J.; Zakrzewski, V. G.; Dapprich, S.; Daniels, A. D.; Strain, M. C.; Farkas, O.; Malick, D. K.; Rabuck, A. D.; Raghavachari, K.; Foresman, J. B.; Ortiz, J. V.; Cui, Q.; Baboul, A.G.; Clifford, S.; Cioslowski, J.; Stefanov, B. B.; Liu, G.; Liashenko, A.; Piskorz, P.; Komaromi, I.; Martin, R. L.; Fox, D. J.; Keith, T.; Al-Laham, M. A.; Peng, C. Y.; Nanayakkara, A.; Challacombe, M.; Gill, P. M. W.; Johnson, B.; Chen, W.; Wong, M. W.; Gonzalez, C.; Pople, J. A. Gaussian, Inc, Wallingford CT, 2004.

[15] Tomasi, J.; Mennucci, B.; Cammi, R., Quantum mechanical continuum solvation models, *Chem. Rev.* **2005**, *105*, 2999-3093, DOI: 10.1021/cr9904009.

[16] Alecu, I. M.; Zheng, J.; Zhao, Y.; Truhlar, D. G., Computational thermochemistry: Scale factor databases and scale factors for vibrational frequencies obtained from electronic model chemistries, *J. Chem. Theory Comput.* **2010**, *6*, 2872-2887, DOI: 10.1021/ct100326h

[17] Gonzales, C.; Schlegel, H. B., An improved algorithm for reaction path following, *J. Chem. Phys.* **1989**, *90*, 2154-2161.

[18] Gonzales, C.; Schlegel, H. B., Reaction path following in mass-weighted internal coordinates, *J. Phys. Chem.* **1990**, *94*, 5523-5527, DOI: 10.1021/j100377a021.

[19] Berman, M. R.; Lin, M. C., Kinetics and mechanism of the methylidyne + molecular nitrogen reaction. Temperature- and pressure-dependence studies and transition-state-theory analysis, *J. Phys. Chem.***1983**, *87*, 3933-3942, DOI: 10.1021/j100243a028.

[20] Holbrook, K. A.; Pilling, M. J.; Robertson, S. H.,Unimolecular Reactions. John Wiley & Sons Ltd, Chichester, England, 1996.

[21] Zhu, L.; Hase, W. L., QCPE Program 644. Quantum Chemistry Program Exchange, Indiana University, Bloomington, IN, 1993.

[22] Shavitt, I., A calculation of the rates of the ortho and para conversions and isotope exchanges in hydrogen, *J. Chem. Phys.* **1959**, *31*, 1359-1367, DOI: http://dx.doi.org/10.1063/1.1730599.

[23] Ramazani, S., Direct-dynamics VTST study of hydrogen or deuterium abstraction and C-C bond formation or dissociation in the reactions of CH_3 + CH_4, CH_3 + CD_4, CH_3D + CD_3, CH_3CH_3 + H and CH_3CD_3 + D, *J. Chem. Phys.***2013**, *138*, 194305-194315, DOI: 10.1063/1.4803862.

[24] Hashemi, S. L.; Ramazani, S., Variational transition state theory with multidimensional tunnelling and kinetic isotope effects in the reactions of C_2H_6, C_2H_5D and C_2D_6 with .CCl_3 to produce $CHCl_3$ and $CDCl_3$, *Mol. Phys.* **2016**, *114*, 2195-2203, DOI: 10.1080/00268976.2016.1190875.

[25] Zheng, J.; Truhlar, D. G., Kinetics of hydrogen-transfer isomerizations of butoxyl radicals, *Phys. Chem. Chem. Phys.* **2010**, *12*, 7782-7793, DOI: 10.1039/B927504E.